Reprinted from JOURNAL OF COMPUTATIONAL PHYSICS
All Rights Reserved by Academic Press, New York and London

Vol. 111, No. 2, April 1994
Printed in Belgium

The Numerical Computation of Connecting Orbits in Dynamical Systems: A Rational Spectral Approach

YINGJIE LIU

Department of Mathematics, The University of Chicago, Chicago, Illinois 60637

AND

LIXIN LIU AND TAO TANG

Department of Mathematics and Statistics, Simon Fraser University, Burnaby, British Columbia, Canada V5A 1S6

Received December 18, 1992; revised July 16, 1993

Structural changes in dynamical systems are often related to the appearance or disappearance of orbits connecting two stationary points (either heteroclinic or homoclinic). To compute the connecting orbits, the boundary value problem which is posed on the real line is frequently replaced by one on a finite interval. Then the problem is solved on the finite interval using appropriate numerical methods. In this work, we use a rational spectral approach to compute the connecting orbits. This method avoids truncating the problem to a finite interval and produces very accurate numerical solutions with a fairly small number of computational points. Numerical examples indicate that the method compares favorably with the existing ones. © 1994 Academic Press, Inc.

1. INTRODUCTION

We consider parametrized dynamical systems of the form

$$u' = f(u, \lambda), \qquad u(t) \in \mathbf{R}^N, \qquad \lambda \in \mathbf{R}^p, \qquad t \in \mathbf{R}, \quad (1.1)$$

where N, $p \geqslant 1$. A solution $u(t)$ of (1.1) at λ is called a connecting orbit if the limits

$$u_- = \lim_{t \to -\infty} u(t), \qquad u_+ = \lim_{t \to \infty} u(t) \qquad (1.2)$$

exist. In the case $u_- = u_+$, the orbit is called a homoclinic orbit; when $u_- \neq u_+$, it is called a heteroclinic orbit. A closed path formed by several heteroclinic orbits is called a heteroclinic cycle. Homoclinic orbits typically arise as limiting cases of periodic orbits which attain infinite period but stay bounded in phase space (see, e.g., [13, 15]). There are also many applications for studying the heteroclinic orbits. For example, the problem of finding traveling wave front solutions of constant speed for nonlinear parabolic equations is equivalent to the problem of finding trajectories that connect two fixed points of an associated system of ordinary differential equations (ODEs). Such a trajectory is an example of a heteroclinic orbit (see, e.g., [10, 11]).

Computation of connecting orbits involves the solution of a boundary value problem on the real line. Therefore, the problem is frequently replaced by one on a finite domain (see, e.g., [2, 3, 9, 12]). The system of ODEs is then solved by the standard ODE boundary value solvers such as the multiple shooting methods and the spline collocation methods [1]. In [10] the connecting orbits are approximated by a series of periodic solutions via a continuation process. These periodic solutions are computed by a spline collocation method with periodic boundary conditions, an integral phase condition, and a pseudo-arclength continuation equation. In [9, 12] Doedel and Friedman discuss a method for computing heteroclinic orbits based on solving boundary value problems. In their computations, the end points are moved away slightly along the eigenvector directions from the fixed points, t is scaled into $[0, 1]$, and the period T is treated as a unknown parameter. Beyn [2, 3] considers the connecting orbits as a boundary value problem on the real line which is truncated into an appropriate finite domain $[T_-, T_+]$. The boundary conditions are determined by projecting the solution into the stable manifold of u_+ near $t = T_+$ and the unstable manifold of u_- near $t = T_-$. In all of these investigations, the reduction of the problems to the finite interval is similar to that in [16].

In this work, we give a new procedure which employs the rational spectral method to compute the connecting orbits. This procedure does not require that the infinite interval be truncated. Further, spectral accuracy can be expected with this approach. Accurate numerical results can be obtained using a small number of grid points.

The organization of the remainder of the paper is as follows. In the next section the rational spectral method is

0021-9991/94 $6.00

introduced. Sections 3 and 4 are devoted to the discussions of boundary condition and phase condition, respectively. Section 5 contains numerical experiments.

2. THE RATIONAL SPECTRAL METHOD

The properties of the rational spectral method have been discussed by several researchers, e.g., Boyd [5, 6], Christov [7], and Weideman [18, 19] with various different types of basis functions. Our rational spectral methods are based on the following basis functions:

$$R_n(t) = \cos(n \cot^{-1}(t)), \qquad n = 0, 1, \ldots. \tag{2.1}$$

The above orthogonal rational functions are merely mapped Chebyshev polynomials, which in turn are the transformed cosines of a Fourier series. With the map $x = t/\sqrt{1+t^2}$, our basis functions, as defined in (2.1), are equal to $T_n(x)$, where the $T_n(x)$ are the usual Chebyshev polynomials. The first five basis functions are

$$R_0(t) = 1, \qquad R_1(t) = \frac{t}{\sqrt{t^2+1}}, \qquad R_2(t) = \frac{t^2-1}{t^2+1},$$
$$R_3(t) = \frac{t(t^2-3)}{(t^2+1)^{3/2}}, \qquad R_4(t) = \frac{t^4-6t^2+1}{(t^2+1)^2}.$$

In general, only the R_n's with n even are truly rational but the others have a square root in the denominator. The orthogonality relation is

$$\int_{-\infty}^{\infty} \frac{1}{1+t^2} R_m(t)\, R_n(t)\, dt = \frac{\pi d_n}{2} \delta_{m,n}, \tag{2.2}$$

where $d_0 = 2$, $d_n = 1$ $(n \geqslant 1)$ and $\delta_{m,n}$ is the Kronecker delta. Thus, if $f(t) \in L^2(\mathbf{R})$ and

$$f(t) = \sum_{n=0}^{\infty} a_n R_n(t),$$

then

$$a_n = \frac{2}{\pi d_n} \int_{-\infty}^{\infty} \frac{1}{1+t^2} f(t)\, R_n(t)\, dt, \qquad n \geqslant 0.$$

Now we consider the use of the rational spectral method to solve (1.1). Let $u = (u_1, \ldots, u_N)^{\mathrm{T}}$ and $f = (f_1, \ldots, f_N)^{\mathrm{T}}$. Substituting the expansions

$$u_i(t) = \sum_{k=0}^{M+1} c_{ik} R_k(t), \qquad 1 \leqslant i \leqslant N, \tag{2.3}$$

into (1.1) gives

$$\sum_{k=0}^{M+1} c_{ik} R_k'(t) = f_i\left(\left(\sum_{k=0}^{M+1} c_{1k} R_k(t), \ldots, \sum_{k=0}^{M+1} c_{Nk} R_k(t)\right)^{\mathrm{T}}, \lambda\right), \quad 1 \leqslant i \leqslant N, \tag{2.4}$$

where M is a given positive integer. The derivatives of $R(t)$, $R'(t)$, can be obtained by direct calculations from (2.1).

2.1. *Rational Pseudospectral Method*

In the practical calculations, it is appropriate to use the pseudospectral method. That is, we assume (2.4) holds at the collocation points $\{t_j\}_{j=1}^{M}$. As mentioned before, our basis functions $R_n(t)$ are mapped Chebyshev polynomials, which suggest that we choose the collocation points as

$$t_j = \cot\left(\frac{j\pi}{M+1}\right), \qquad 1 \leqslant j \leqslant M. \tag{2.5}$$

Further, due to the nature of the rational spectral functions we can add two collocation points, $t_0 = +\infty$ and $t_{M+1} = -\infty$. Using the relation

$$u_i(t_j) = \sum_{k=0}^{M+1} c_{ik} \cos\left(\frac{kj\pi}{M+1}\right), \qquad 0 \leqslant j \leqslant M+1, \tag{2.6}$$

we have

$$c_{ik} = \frac{2}{(M+1)\,\bar{c}_k} \sum_{m=0}^{M+1} \bar{c}_m^{-1} u_i(t_m) \cos\left(\frac{mk\pi}{M+1}\right), \quad 0 \leqslant k \leqslant M+1, \tag{2.7}$$

where $\bar{c}_m = 2$ if $m = 0$ or $M+1$ and $\bar{c}_m = 1$ if $1 \leqslant m \leqslant M$. Noting that

$$R_k'(t_j) = k \sin^2\left(\frac{j\pi}{M+1}\right) \sin\left(\frac{kj\pi}{M+1}\right), \tag{2.8}$$

we have, for $1 \leqslant j \leqslant M$,

$$u_i'(t_j) = \sum_{k=0}^{M+1} c_{ik} k \sin^2\left(\frac{j\pi}{M+1}\right) \sin\left(\frac{kj\pi}{M+1}\right)$$
$$= \frac{2}{M+1} \sin^2\left(\frac{j\pi}{M+1}\right) \sum_{k,m} \frac{k}{\bar{c}_k \bar{c}_m} \cos\left(\frac{mk\pi}{M+1}\right) \times \sin\left(\frac{kj\pi}{M+1}\right) u_i(t_m). \tag{2.9}$$

Note that $u(t_0) = u_+$, $u(t_{M+1}) = u_-$. The above result, together with

$$u_i'(t_j) = f_i(u(t_j), \lambda), \qquad 1 \leqslant i \leqslant N, \qquad 1 \leqslant j \leqslant M, \tag{2.10}$$

yields NM equations for the NM unknowns $u_i(t_j)$, $1 \leqslant i \leqslant N$, $1 \leqslant j \leqslant M$. The main advantage of the pseudospectral method is that it allows one to work in the physical space rather than the coefficient space. Thus it is possible to handle nonlinearities very efficiently, without the convolution sums introduced by the pure spectral method.

2.2. *Rational Spectral Method*

Applying the collocation points as given in (2.5) to (2.4) gives, for $1 \leqslant j \leqslant M$, $1 \leqslant i \leqslant N$,

$$\sum_{k=0}^{M+1} k \sin^2\left(\frac{j\pi}{M+1}\right) \sin\left(\frac{kj\pi}{M+1}\right) c_{ik} = f_i\left(\left(\sum_{k=0}^{M+1} c_{1k} \cos\left(\frac{kj\pi}{M+1}\right), \ldots, \sum_{k=0}^{M+1} c_{Nk} \times \cos\left(\frac{kj\pi}{M+1}\right)\right)^{\mathrm{T}}, \lambda\right). \tag{2.11}$$

The above system gives NM equations. We need another $2N$ conditions, which are given by (1.2), so that the $N(M+2)$ unknowns c_{ik}, $1 \leqslant i \leqslant N$, $0 \leqslant k \leqslant M+1$, can be obtained. This will be discussed in Subsection 3.4.

In this work, we solve (1.1)–(1.2), using the spectral method (2.11). It is also possible to obtain numerical solutions using the pseudospectral method as described in Subsection 2.1. A comparison between the rational pseudospectral method and the rational spectral method will be given for Example 1 in Section 5.

2.3. *Scaling Factor*

It has been noted in [5, 6, 17, 18] that for the rational and the Hermite spectral methods we have the freedom to stretch the t variable according to $t \leftrightarrow Lt$. The scaling factor L can be selected to optimize accuracy. A detailed analysis for choosing the scaling factor with the rational and the Hermite approaches was given in [5, 17], respectively. In solving (1.1) and (1.2), the use of a scaling factor L yields the equation

$$Lu'(t) = f(u, \lambda). \tag{2.12}$$

We then solve (2.12) subject to the boundary conditions (1.2). We show how to choose a scaling factor in Section 5.

3. BOUNDARY CONDITIONS

In the present work we assume that both u_- and u_+ are hyperbolic fixed points. Let $M_S(u_\pm)$ and $M_U(u_\pm)$ be stable and unstable manifolds at u_- and u_+, respectively, with corresponding dimensions $m_{\pm S}, m_{\pm U}$. If there exists exactly one orbit, then $m_{-U} + m_{+S} = N+1$. When $m_{-U} + m_{+S} < N+1$, the connect orbit is not structurally stable and $p = N+1-(m_{+U}+m_{+S})$ free parameters are needed to stabilize the system. For ease of exposition we consider in this work the case that there is only one free parameter, i.e., $p=1$, which is always true for the homoclinic case and also true for many heteroclinic cases. For $p>1$, appropriate projection boundary conditions can be used to form a well-posed problem.

We now summarize some of the well-known boundary conditions for computing the connecting orbits.

3.1. *The Periodic Boundary Condition*

The periodic boundary conditions are defined by

$$u(T_-) = u(T_+). \tag{3.1}$$

This type of boundary condition is very natural for computing periodic solutions of a dynamical system and is used in the software package AUTO [8, 10]. In this package, the homoclinic orbits are approximated by the periodic solutions at very high period. This is because for homoclinic orbits, there exist nearby periodic solutions. However, it is not necessarily true for the heteroclinic case and the periodic boundary conditions may not be appropriate.

3.2. *The Eigenvector Method*

This method was investigated in [9, 12]. It is clear that

$$f(u_-, \lambda) = 0, \qquad f(u_+, \lambda) = 0, \tag{3.2}$$

since $u_\pm$ are the fixed points. Suppose that $f_u(u_-, \lambda)$ has n_- distinct positive eigenvalues, $f_u(u_+, \lambda)$ has n_+ distinct negative eigenvalues, and these eigenvalues and their corresponding eigenvectors satisfy

$$f_u(u_\pm, \lambda)\, v_i^\pm = \mu_i^\pm v_i^\pm, \qquad \|v_i^\pm\| = 1, \qquad i = 1, \ldots, n_\pm. \tag{3.3}$$

Then the boundary conditions for (1.1) are defined by

$$u(T_-) = u_- + \varepsilon_- \sum_{i=1}^{n_-} c_i^- v_i^-, \qquad \sum_{i=1}^{n_-} (c_i^-)^2 = 1, \tag{3.4}$$

$$u(T_+) = u_+ + \varepsilon_+ \sum_{i=1}^{n_+} c_i^+ v_i^+, \qquad \sum_{i=1}^{n_+} (c_i^+)^2 = 1, \tag{3.5}$$

where $\varepsilon_\pm, c_i^\pm \in \mathbf{R}$.

3.3. *The Projection Method*

The projection boundary conditions (also known as asymptotic boundary conditions) are used by Beyn [2, 3]. The method involves finding the unstable subspace $Y_-^U(\lambda)$ at u_- and the stable subspace $Y_+^S(\lambda)$ at u_+ and the boundary condition takes the form

$$u(T_-) - u_- \in Y_-^U(\lambda), \qquad u(T_+) - u_+ \in Y_+^S(\lambda). \tag{3.6}$$

Suppose that the rows of matrices $L_{-S}(\lambda) \in \mathbf{R}^{n_- \times N}$, $L_{+U}(\lambda) \in \mathbf{R}^{n_+ \times N}$ span the stable subspace of $f_u^T(u_-, \lambda)$ and unstable subspace of $f_u^T(u_+, \lambda)$, respectively, then the projection boundary condition can be written as

$$L_{-S}(\lambda)(u(T_-) - u_-) = 0, \qquad L_{+U}(\lambda)(u(T_+) - u_+) = 0. \tag{3.7}$$

The projection boundary conditions have better convergence properties than the periodic boundary conditions, but one would require that the connecting curves be isolated.

3.4. *The Exact Boundary Condition*

In our computation, we introduce a different type of numerical boundary condition due to the nature of the rational spectral functions. Unlike the above-mentioned numerical boundary conditions, the following method does not require that the infinite interval be truncated. For the boundary conditions (1.2), noting that

$$\lim_{t\to-\infty} R_k(t)=(-1)^k, \qquad \lim_{t\to\infty} R_k(t)=1,$$
$$0\leqslant k\leqslant M+1, \tag{3.8}$$

we obtain that

$$u_- = \sum_{k=0}^{M+1} (-1)^k c_{ik}, \qquad u_+ = \sum_{k=0}^{M+1} c_{ik}. \tag{3.9}$$

Equations (2.11) and (3.9) consist of $N(M+2)$ equations, $N(M+2)$ unknowns c_{ik} $(1\leqslant i\leqslant N, 0\leqslant k\leqslant M+1)$, and one free parameter λ.

4. PHASE CONDITIONS

If $u(t)$ is a solution of (1.1)–(1.2), then for any constant $t_0\in\mathbf{R}$, $u(t+t_0)$ is also a solution. To remove the indeterminacy it is necessary to add an appropriate constraint called a *phase condition* in analogy with the periodic case. The possible phase conditions are normally of integral or differential forms.

4.1. *The Integral Form*

In [9] the phase condition is obtained by requiring that the current heteroclinic orbit look like the previously computed orbit as much as possible. More precisely, let $\hat{u}(t)$ denote the previous orbit on a branch of heteroclinic orbits. Let $\bar{u}(t+\sigma)$ be the continuum from which the current orbit is to be selected. Since $\|u'(t)\|\to 0$ as $t\to\pm\infty$, a good measure of how close $\bar{u}$ and $\hat{u}$ are is the integral

$$D(\sigma)\equiv\int_{-\infty}^{\infty} \|\bar{u}'(t+\sigma)-\hat{u}'(t)\|^2\,dt. \tag{4.1}$$

The necessary condition for a minimum is $D'(\sigma_*)=0$. With $u(t)\equiv\bar{u}(t+\sigma_*)$ the required phase condition can be written as

$$\int_{-\infty}^{\infty} \langle u'(t)-\hat{u}'(t), u''(t)\rangle\,dt=0. \tag{4.2}$$

In the above, $\langle\cdot,\cdot\rangle$ is the l^2 inner product, and $\|\cdot\|$ is the corresponding norm. An alternative approach in [8, 10] is to minimize the function

$$E(\sigma)=\int_{-\infty}^{\infty} \|u(t+\sigma)-\hat{u}(t)\|^2\,dt. \tag{4.3}$$

Letting $E'(0)=0$ yields the phase condition

$$\int_{-\infty}^{\infty} \langle u(t)-\hat{u}(t), u'(t)\rangle\,dt=0. \tag{4.4}$$

4.2. *The Differential Form*

A classical phase condition (see, e.g., [2]) is to require

$$\langle u(0)-\hat{u}(0), \hat{u}'(0)\rangle=0. \tag{4.5}$$

This phase condition fixes $u(0)$ in a hyperplane through $\hat{u}(0)$ and orthogonal to $\hat{u}'(0)$. From a numerical point of view, the condition (4.5) is in general not as reliable as the conditions (4.2) and (4.4).

4.3. *A New Phase Condition*

Now we introduce a new phase condition which does not require the information at the previous continuation step and which is more appropriate when using the rational spectral method. We choose current solution $u(t)$ so that the fastest changing region for $u(t)$ is in the location where the collocation points are the most densely allocated. For our choice of the collocation points, this location is around $t=0$. This means that $\|u'(t)\|$ should reach its maximum at $t=0$. Therefore,

$$\left.\frac{d\,\|u'(t)\|}{dt}\right|_{t=0} = \left.\frac{d\,\|f(u,\lambda)\|}{dt}\right|_{t=0} = 0. \tag{4.6}$$

From (4.6), we obtain the phase condition

$$\langle f(u(0),\lambda), f'_u(u(0),\lambda)\,u'(0)\rangle=0. \tag{4.7}$$

Note that

$$u_i(0)=\sum_{k=0}^{[(M+1)/2]} (-1)^k c_{i,2k}, \qquad 1\leqslant i\leqslant N,$$
$$u_i'(0)=\sum_{k=0}^{[M/2]} (-1)^k (2k+1)\, c_{i,2k+1}, \qquad 1\leqslant i\leqslant N,$$

where $[a]$ denotes the integral part of a. Hence, (4.7) gives an equation for c_{ik}, which can be used to determine a unique solution of (1.1)–(1.2).

In the case when the maximum of $\|u'\|$ is more than one, the new phase condition (4.7) can still be used. Since when

$|t|$ is large $\|u'\|$ decays to zero and therefore its maximums are located in a fixed interval in which the solution u changes quite rapidly. The condition (4.7) will fix one of the (local) maximums/minimums at the origin.

5. NUMERICAL RESULTS

In order to illustrate the numerical method described in Sections 2–4, we consider two examples. In our numerical computation, the subroutine DNEQN from IMSL is used to solve the nonlinear system of equations. The computations are done on a SUN 4/670 with double precision.

EXAMPLE 1. The Huxley equation,

$$w_t = w_{zz} + f(w, a), \qquad z \in \mathbf{R}, \qquad t > 0, \tag{5.1}$$

$$f(w, a) \equiv w(1-w)(w-a), \qquad a \in (0, 1). \tag{5.2}$$

We look for traveling wave solutions to (5.1)–(5.2) of the form $w(z, t) = u(z + bt)$, where b is the wave speed. This gives the first-order ODE system

$$\frac{du_1(x)}{dx} = u_2(x), \tag{5.3}$$

$$\frac{du_2(x)}{dx} = bu_2(x) - f(u_1(x), a), \tag{5.4}$$

where $x = z + bt$. If $a = 0.5$ and $b = 0$ then (5.3)–(5.4) has a family of periodic orbits of increasing period. In the limit, as the period goes to infinity, the orbits approach a heteroclinic cycle with rest points (0, 0) and (1, 0). The first of the two heteroclinic orbits has the exact representation

$$u_1(x) = \frac{\exp(x/\sqrt{2})}{1 + \exp(x/\sqrt{2})}, \qquad u_2(x) = \frac{du_1(x)}{dx}. \tag{5.5}$$

The second heteroclinic connection is obtained by reflecting the phase plane representation of the first with respect to the horizontal axis $u_2 = 0$. Since this test problem has (5.5) as an exact solution, it is useful to test our spectral method.

As mentioned in Section 2, a scaling factor L is useful to optimize computational accuracy. In Fig. 1 we plot the computed u_1 with $M = 29$ and $L = 2$, 1, 0.5, and 0.1, respectively. It is observed that if L is not carefully chosen then numerical oscillations are present. Graphically it is seen that a reasonable choice of L in this case is in the region [0.1, 0.5], since smooth curves are obtained if L is in this interval. It was found in [5, 6] that the accuracy is not very sensitive to L in the neighborhood of the optimum L. Therefore, it is safe to use any L in this "trusted" region. Based on this observation, for any given M we can obtain a corresponding interval from which we can choose any value as L.

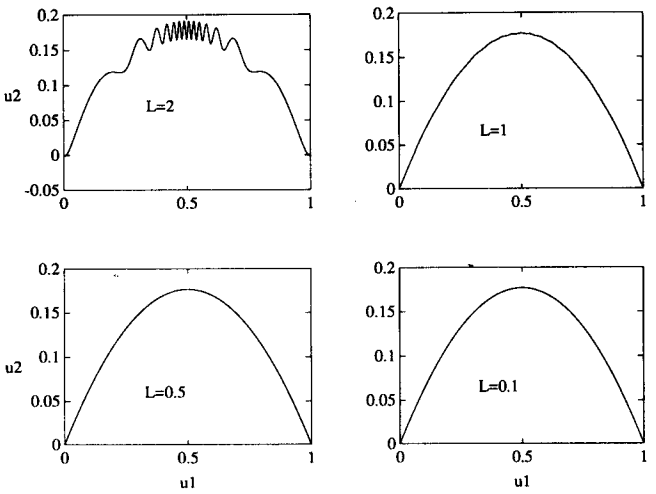

FIG. 1. Numerical solutions of u_1 with $M = 29$ and various values of L.

For Example 1, the exact representation of the two branches is $b = \pm\sqrt{2}\,(a - 0.5)$. Therefore in the case $a = 0.5$ the exact value of b is 0. Figure 2 shows the numerical values of $|b|$ against the number of collocation points, M; the corresponding scaling factors used are shown in Fig. 3. It is noted that if $M > 10$ then the scaling factors used are almost independent of M. The spectral accuracy can be clearly seen from Fig. 2. For a given M, we define the numerical errors as

$$\text{error} \equiv \max_{1 \le j \le M} \|u(t_j) - U(t_j)\|, \tag{5.6}$$

where $u = (u_1, u_2)^T$ is the exact solution given in (5.5), U is the numerical solution, $\|\cdot\|$ is the standard l^2 norm. The numerical error is plotted in Fig. 4, which also shows a spectral convergence rate. Figure 5 shows the numerical results

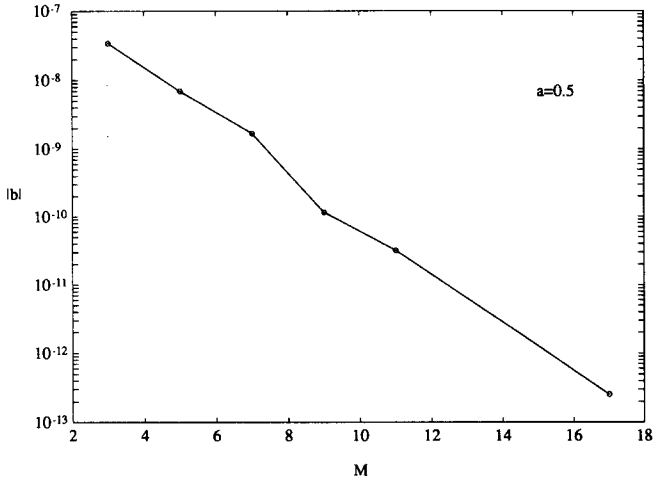

FIG. 2. Numerical solutions of $|b|$ in the case $a = 0.5$ with different M; the exact value of b at $a = 0.5$ is 0.

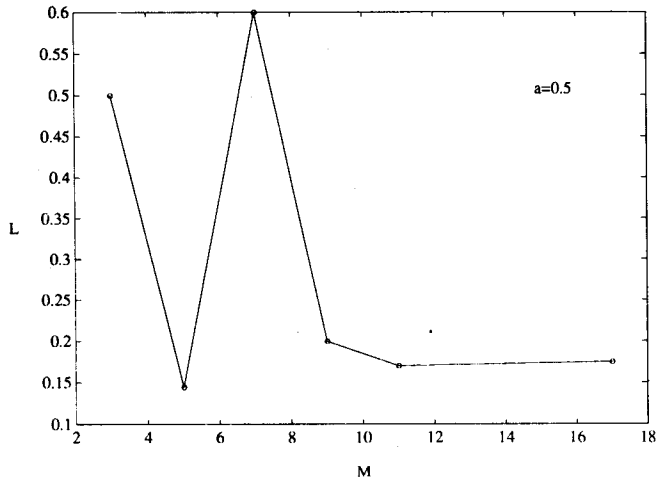

FIG. 3. The variation of the scaling factor L with M for $a = 0.5$.

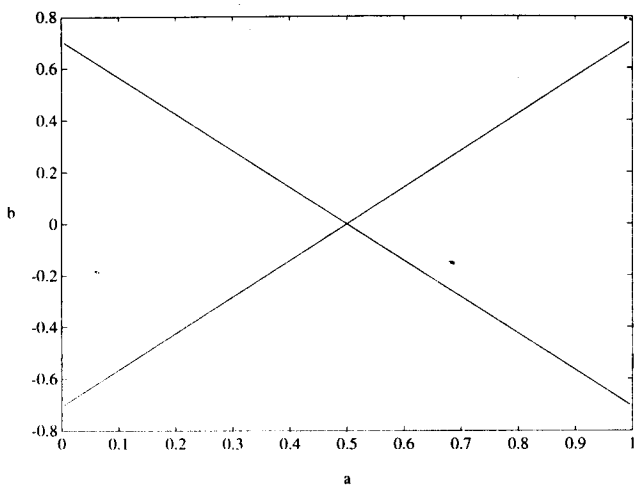

FIG. 5. The two branches of traveling wave solutions to the Huxley equation. The number of collocation points used is 29.

of the two branches of traveling wave front solutions to (5.1)–(5.2). This figure is graphically indistinguishable from the analytical representation $b = \pm\sqrt{2}\,(a - 0.5)$. It is noted that Doedel and Friedman [9] also obtained the same results by using AUTO with total 200 collocation points. In Fig. 6 we compare the methods used in [9] and in the present paper by plotting the numerical errors of b. The AUTO results are obtained by using 25 mesh intervals, four orthogonal points on each mesh interval and adaptive mesh selection, and thus 100 collocation points in total. The spectral results are obtained by use of 29 collocation points with a constant scaling factor $L = 0.181$.

The solution procedure with AUTO is as follows. We begin by using the exact periodic solution with period $T = 5$ ($T = T_+ - T_-$) as starting values. AUTO used 90 continuation steps, with 68 s CPU time, to obtain approximate heteroclinic solution with $T = 5000$. Then 46 continuation steps, with 31 s CPU time, were used to obtain the lower half branch ($0.5 \leqslant a < 1$). The total CPU time used is about 100 s. The rational spectral method requires 46 s CPU time to compute the same branch using 50 different values of a.

In order to compare the efficiency and accuracy of rational spectral method and rational pseudospectral method we also present numerical results using the rational pseudospectral method as described in Subsection 2.1. It can be seen from Fig. 6 that the results using the rational pseudospectral method are comparable with those obtained with AUTO but are less accurate than those obtained with

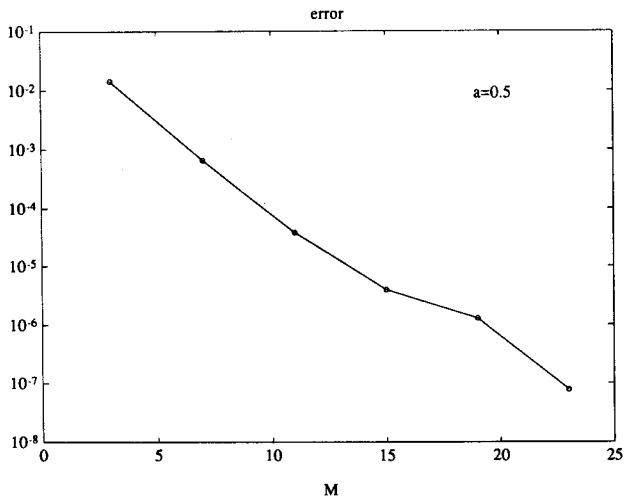

FIG. 4. The maximum errors between the exact and the numerical solutions of u_1.

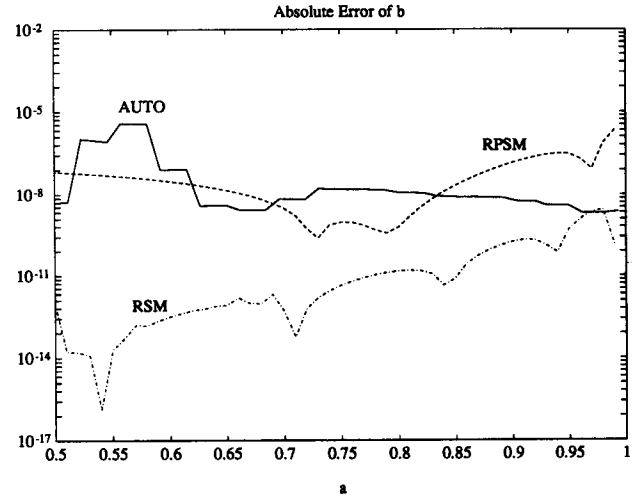

FIG. 6. The comparison between the AUTO results (solid line), pseudospectral (dashed line), and the spectral solutions (dot-dashed line). The number of collocation points used are 100 for AUTO and 29 each for the rational pseudospectral method (RPSM) and the rational spectral method (RSM). The scaling factor used for RPSM and RSM is 0.181.

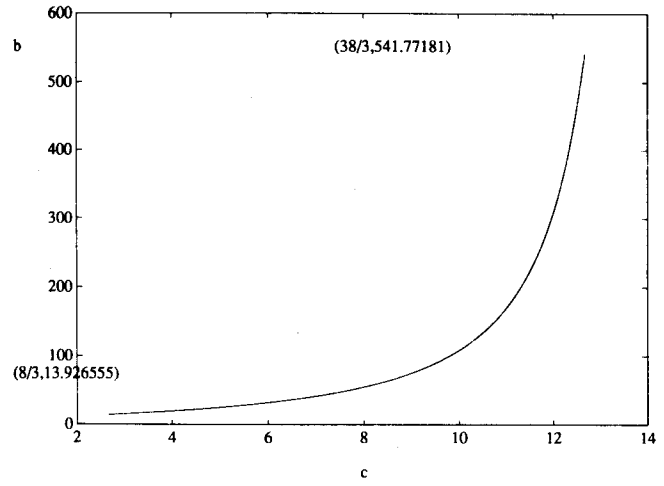

FIG. 7. The values of b for a branch of homoclinic orbits in the Lorenz equation.

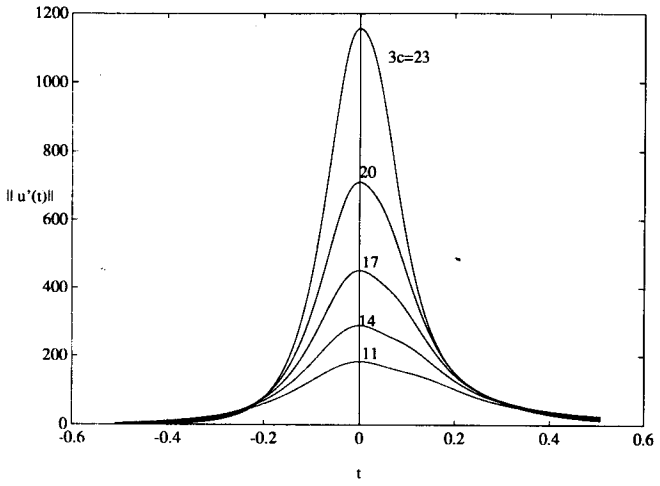

FIG. 9. The variation of $\|u'\|$. The phase condition is to fix the maximum point of $\|u'\|$ at the origin.

the rational spectral method. However, the pseudospectral method used only 23 s CPU time and, as expected, is more efficient than both AUTO and the pure spectral method.

EXAMPLE 2. The Lorenz equation,

$$x' = a(y - x), \qquad y' = bx - y - xz, \qquad z' = -cz + xy. \tag{5.7}$$

When $(a, c) = (10, \frac{8}{3})$, the Lorenz equation has a homoclinic solution. The stationary point is (0, 0, 0), and there is one positive eigenvalue and two negative eigenvalues in the linearized ODE system at the origin. Therefore, the dimension of the unstable and stable subspaces are one and two, respectively. At the Lorenz values $(a, c) = (10, \frac{8}{3})$, we compute the homoclinic orbit connecting the origin with itself and the b value using 29 collocation points. The computed value for b in this case is 13.926555 which is in very good agreement with $b = 13.926557$ obtained by Beyn [3]. Figure 7 shows the values of b along the branch as obtained by our procedure. The curve is in good agreement with Beyn's. Furthermore, the phase curves are plotted in Fig. 8, which are found graphically indistinguishable from Beyn's results. Finally, we show how the new phase condition introduced in Section 4 works. In Fig. 9, we plot $\|u'\|$ against t, with $a = 10$ and several values of c. It is observed that the new phase condition fixes the maximum values of $\|u'\|$ at the origin, which ensures the uniqueness of the solution.

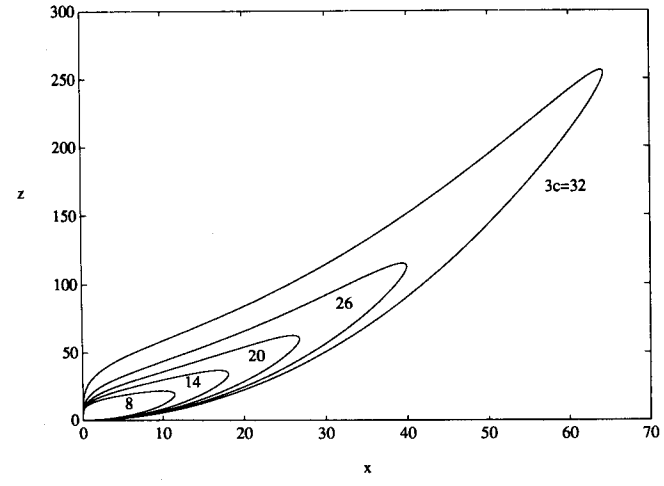

FIG. 8. Projection of homoclinic orbits in the Lorenz equations into xz plane with $3c = 8$, 14, 20, 26, and 32.

6. CONCLUSIONS

In this work we have developed a numerical technique based on rational spectral methods for computing connecting orbits for the dynamical systems (1.1), which avoids the difficulty in satisfying the boundary conditions at infinity. Numerical results indicate that the new technique can produce very accurate numerical solutions with a small number of collocation points. In the conclusion we give a summary of the points we have raised in the present work.

- It is well known that spectral methods are very efficient for solving differential equations with smooth solutions (see, e.g., [14]). That is, the smoothness of exact solutions plays an important role for the convergent rates of spectral methods. For the dynamical systems (1.1), if $f \in C^\infty(\mathbf{R}^N \times \mathbf{R}^P)$, which is the case in the Huxley equation and the Lorenz equation, then the solutions $u \in C^\infty$. Therefore, it is reasonable to use spectral methods to solve (1.1) whenever the given function f is smooth.

- The rational pseudospectral/spectral methods described in Section 2 are very useful in obtaining accurate

numerical solutions for the dynamical systems (1.1)–(1.2). The main advantage of using the rational approach is that the procedure does not require that the infinite interval be truncated.

• The new phase condition (4.7) is found to be more appropriate when using the rational spectral approach. The numerical calculations indicate that Newton's method, together with the pseudospectral/spectral methods and the new phase condition, converges very quickly.

• In the calculations, it is found that a scaling factor is useful to optimize accuracy. Like [4] we obtained the optimum scaling factor through trial and error. It remains to be investigated if we can find a theoretical method to determine the optimum scaling factor.

ACKNOWLEDGMENTS

The authors are grateful to the referees and Dr. Erik Van Vleck for helpful comments and suggestions on an earlier version of this paper. The research of T. Tang was supported by the Natural Sciences and Engineering Research Council of Canada (NSERC Operating Grant OGP0105545).

REFERENCES

1. U. Ascher, R. M. M. Mattheij, and R. D. Russell, *Numerical Solution of Boundary Value Problems for Ordinary Differential Equations* (Prentice–Hall, Englewood Cliffs, NJ, 1988).
2. W.-J. Beyn, "Global Bifurcations and Their Numerical Computation," in *Continuation and Bifurcations: Numerical Integration Techniques and Applications, Leuven*, NATO ASI Series, edited by D. Roose (Plenum, New York/London, 1989).
3. W.-J. Beyn, *IMA J. Numer. Anal.* **10**, 79 (1990).
4. G. Birkhoff and G. Fix, "Accurate Eigenvalue Computation for Elliptic Problems," in *Numerical Solution of Field Problems in Continuum Physics, Providence*, RI, SIAM-AMS Proceedings, Vol. 2 (Am. Math. Soc., Providence, RI, 1970), p. 111.
5. J. Boyd, *J. Comput. Phys.* **45**, 43 (1982).
6. J. Boyd, *J. Comput. Phys.* **69**, 112 (1987).
7. C. I. Christov, *SIAM J. Appl. Math.* **42**, 1337 (1982).
8. E. J. Doedel, *Congr. Numer.* **30**, 265 (1981).
9. E. J. Doedel and M. J. Friedman, *J. Comput. Appl. Math.* **26**, 159 (1989).
10. E. J. Doedel and J. P. Kernevez, Applied Maths. Technical Report, Caltec, 1986 (unpublished).
11. P. C. Fife, *Mathematical Aspects of Reacting and Diffusing Systems*, Lecture Notes in Biomathematics, Vol. 28 (Springer-Verlag, New York/Berlin, 1979).
12. A. J. Friedman and E. J. Doedel, *SIAM J. Numer. Anal.* **28**, 789 (1991).
13. P. Glendinning, "Global Bifurcations in Flows," in *LMS Lecture Note Series*, Vol. 127 (Cambridge Univ. Press, 1988), p. 120.
14. D. Gottlieb and S. Orszag, *Numerical Analysis of Spectral Methods: Theory and Applications*, CBMS-NSF Regional Conference Series in Applied Mathematics, Vol. 26 (SIAM, Philadelphia, 1977).
15. J. Guckenheimer and P. Holmes, *Nonlinear Oscillations, Dynamical Systems, and Bifurcations of Vector Fields*, Applied Mathematical Sciences, Vol. 42 (Springer-Verlag, New York/Berlin, 1983).
16. M. Lentini and H. B. Keller, *SIAM J. Numer. Anal.* **17**, 557 (1980).
17. T. Tang, *SIAM J. Sci. Comput.* **14**, 594 (1993).
18. J. A. C. Weideman, *Numer. Math.* **61**, 409 (1992).
19. J. A. C. Weideman, private communication, 1992.

Printed by Catherine Press, Ltd., Tempelhof 41, B-8000 Brugge, Belgium